Electronic Supplementary Material (ESI) for Journal of Materials Chemistry A.

Controllable Synthesis of Layered $K_{0.296}Mn_{0.926}O_2$ to Assemble 2.4 V Aqueous Potassium-Ion Supercapacitors for Double High Device

Xijun Wei,[a] Bin Zhang,[b] Minhui Liao,[c] Peng Xiao,[*a] Xiaoyuan Zhou,[b] Yunhuai Zhang,[a] Jiangtao Liu[*c]

[a] *College of Chemistry and Chemical Engineering, Chongqing University, Chongqing 400044, China*

[b] *Analytical and Testing Center of Chongqing University, Chongqing 400044, China*

[c.] *State Key Laboratory of Advanced Chemical Power Sources, Guizhou Meiling Power Sources Co. Ltd., Zunyi, Guizhou 563003, China*

Notes

The authors declare no competing financial interest.

Figure captions

Figure.S1. (a) (b) SEM images of the MnO_2 and as-prepared $K_{0.296}Mn_{0.926}O_2$, respectively; (c) AFM image of the as-prepared $K_{0.296}Mn_{0.926}O_2$; (d) Obtained 3D image from the AFM image in Figure S1c.

Figure.S2. Powder XRD patterns of the commercial MnO_2.

Figure.S3. XPS spectra analysis for the K 2p (a) and O 1s (b) of as-prepared $K_{0.296}Mn_{0.926}O_2$, respectively.

Figure.S4. XPS spectra of MnO_2(a) and O 1s (b), respectively.

Figure.S5. The EDX spectrum of $K_{0.296}Mn_{0.926}O_2$.

Figure.S6. (a) CV curves of commercial MnO_2 at the scan rate between 10 and 80 mV s^{-1}; (b) Galvanostatic charge-discharge curves of commercial MnO_2 at the current densities between 1 and 5 A g^{-1}.

Figure.S7. Density of states (DOS) of the MnO_2 and as-prepared $K_{0.296}Mn_{0.926}O_2$ using density functional theory (DFT)

Figure.S8. CV curves of MnO_2 and as-prepared $K_{0.296}Mn_{0.926}O_2$ at the scan rate between 1 and 9 mV s^{-1}, respectively.

Figure.S9. (a), (c) The contribution of the different energy storage mechanism of the MnO_2 and $K_{0.296}Mn_{0.926}O_2$ at 9 mV s^{-1}; (b), (d) Percentage of diffusion-controlled and surface-capacitance for the MnO_2 and $K_{0.296}Mn_{0.926}O_2$ at various scan rates, respectively.

Figure S10. (a), (b) The SEM images of MnO_2 after cycling; (c), (d) EDS-mapping of Figure S9(b).

Figure S11. (a), (b) The SEM images of $K_{0.296}Mn_{0.926}O_2$ after cycling.

Figure S12. The XRD spectrum of $K_{0.296}Mn_{0.926}O_2$ after cycling.

Figure.S13. CV curves of MnO_2//AC at different potentials at a scan rate of 20 mV s^{-1}.

Figure.S14. (a) CV curves of MnO_2//AC at the scan rate between 10 and 80 mV s^{-1}; (b) Galvanostatic charge-discharge curves of MnO_2//AC at the current densities between 1 and 5 A g^{-1}.

Figure. S15. (a), (b) The computational models of bulk MnO_2 and $K_{0.296}Mn_{0.926}O_2$, respectively.

Table S1. The comparative table of morphology, specific surface areas and average pore diameters of our prepared products with previously reported literature.

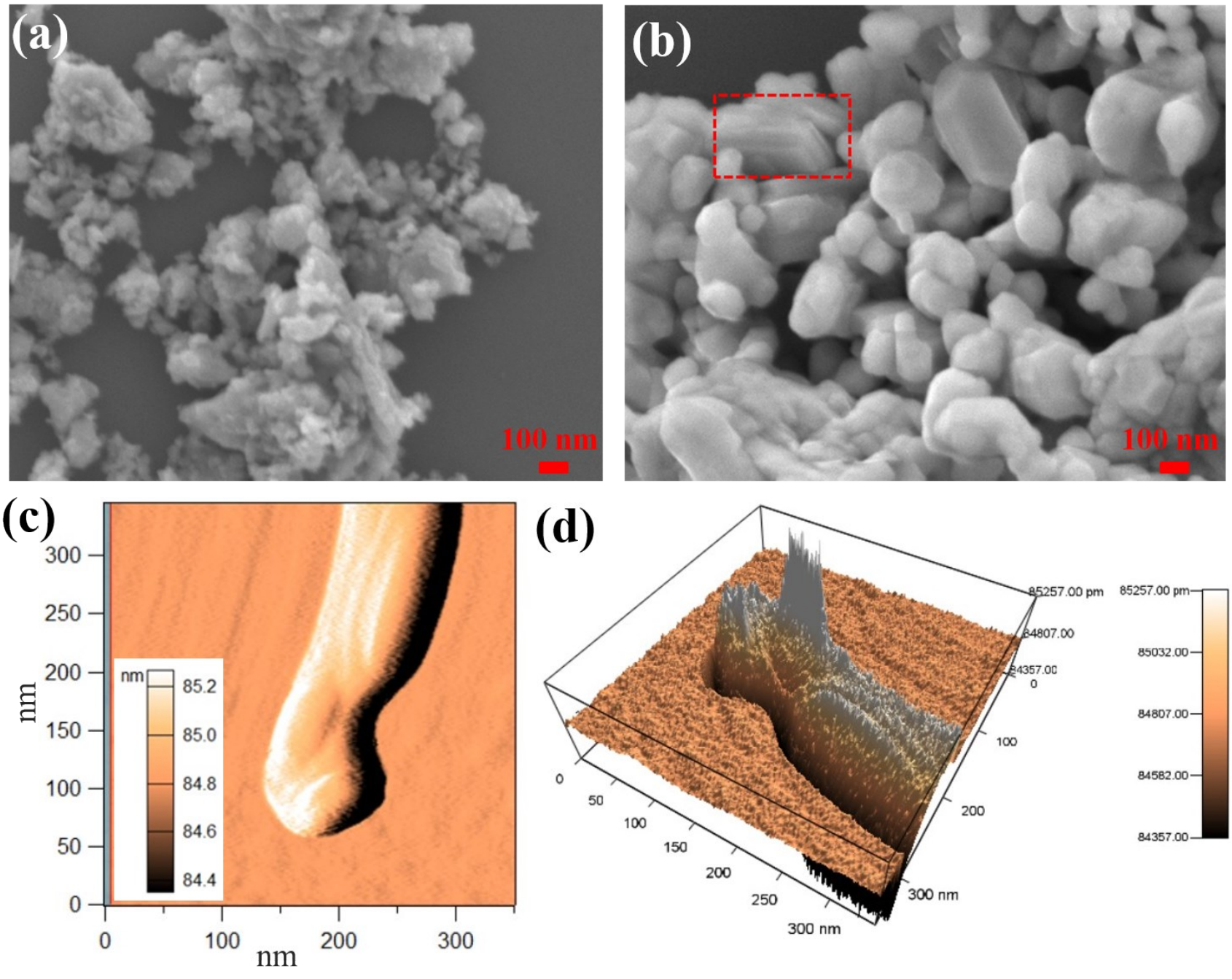

Figure.S1. (a) (b) SEM images of the MnO_2 and as-prepared $K_{0.296}Mn_{0.926}O_2$, respectively; (c) AFM image of the as-prepared $K_{0.296}Mn_{0.926}O_2$; (d) Obtained 3D image from the AFM image in Figure S1c.

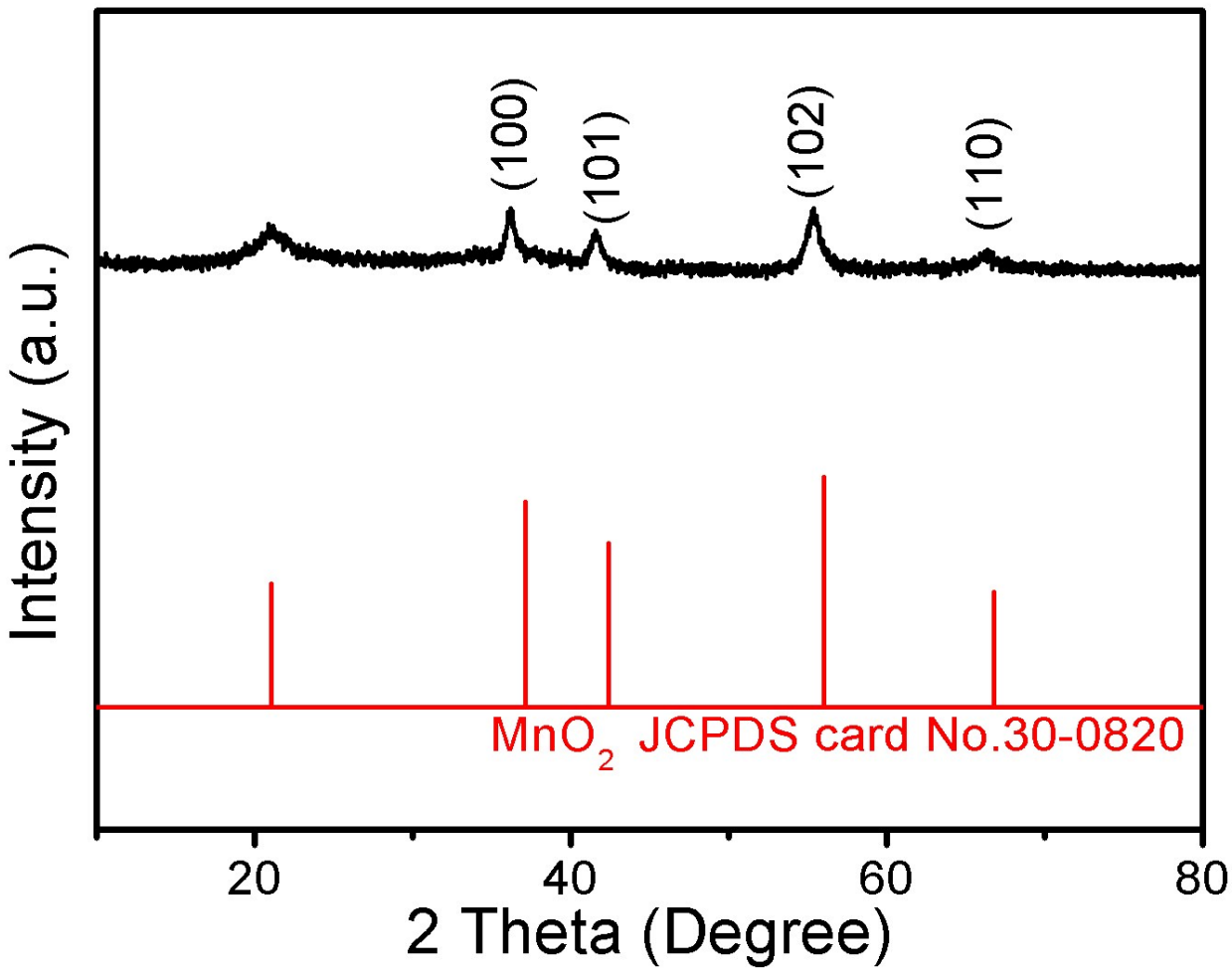

Figure.S2. Powder XRD pattern of the commercial MnO_2.

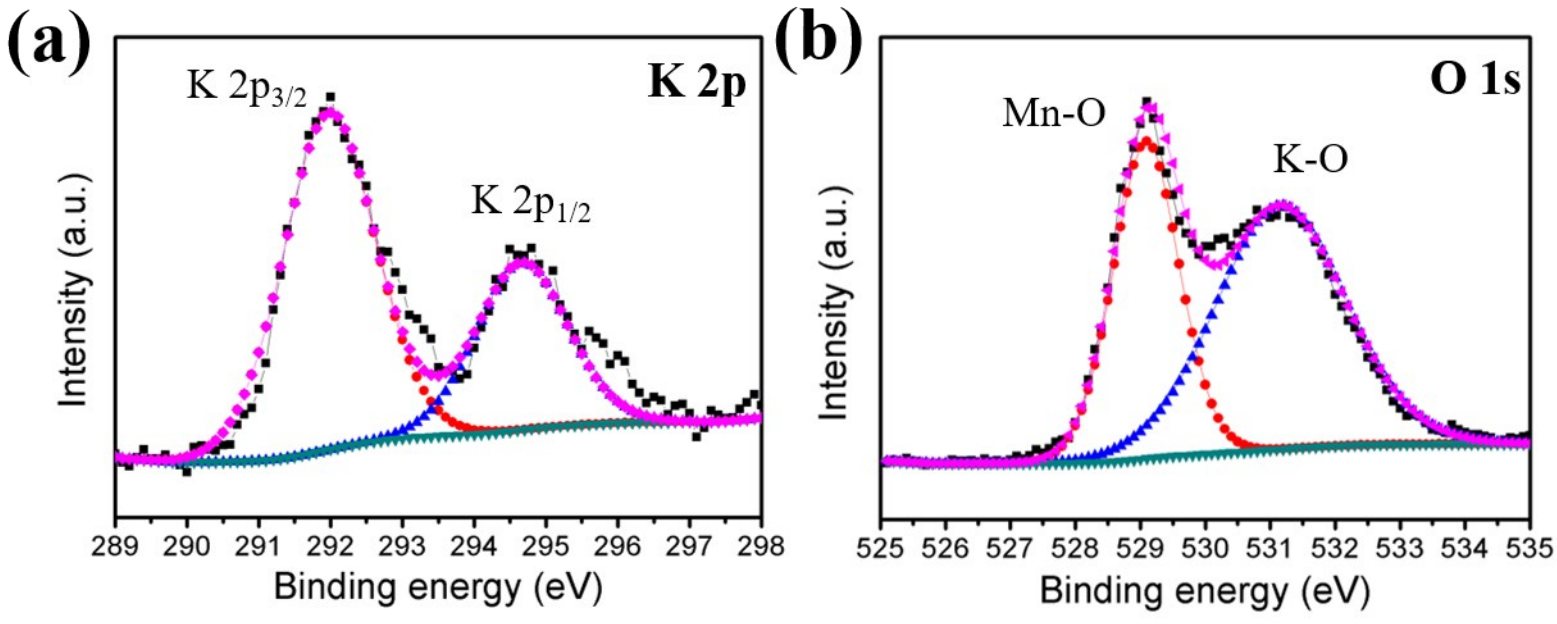

Figure.S3. XPS spectra analysis for the K 2p (a) and O 1s (b) of as-prepared $K_{0.296}Mn_{0.926}O_2$, respectively.

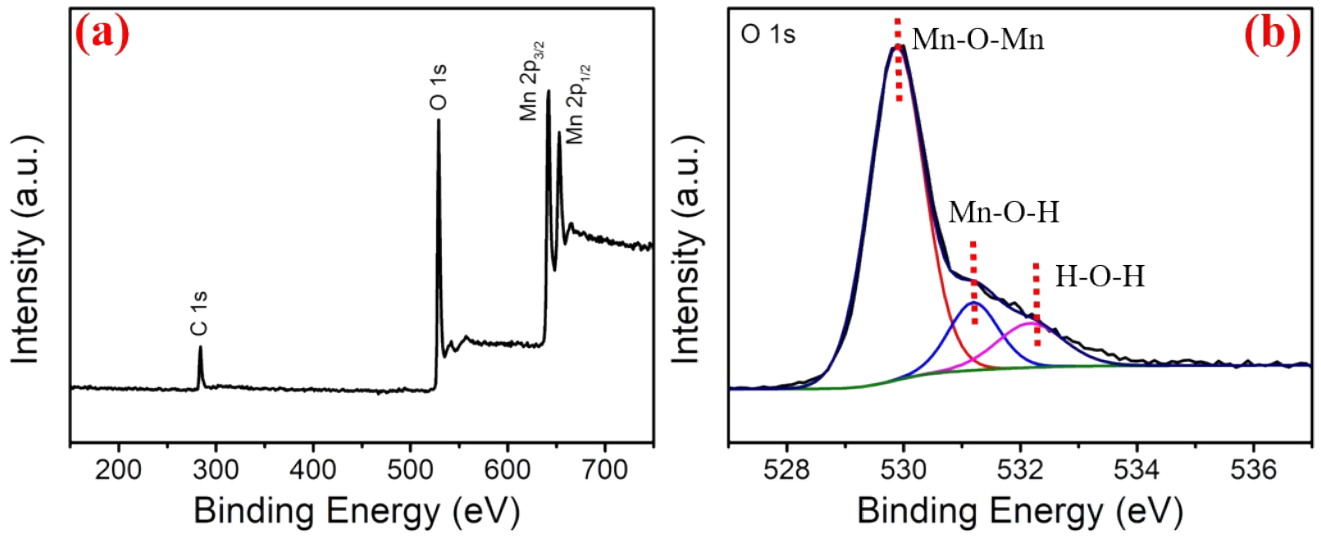

Figure.S4. XPS spectra of MnO_2(a) and O 1s (b), respectively.

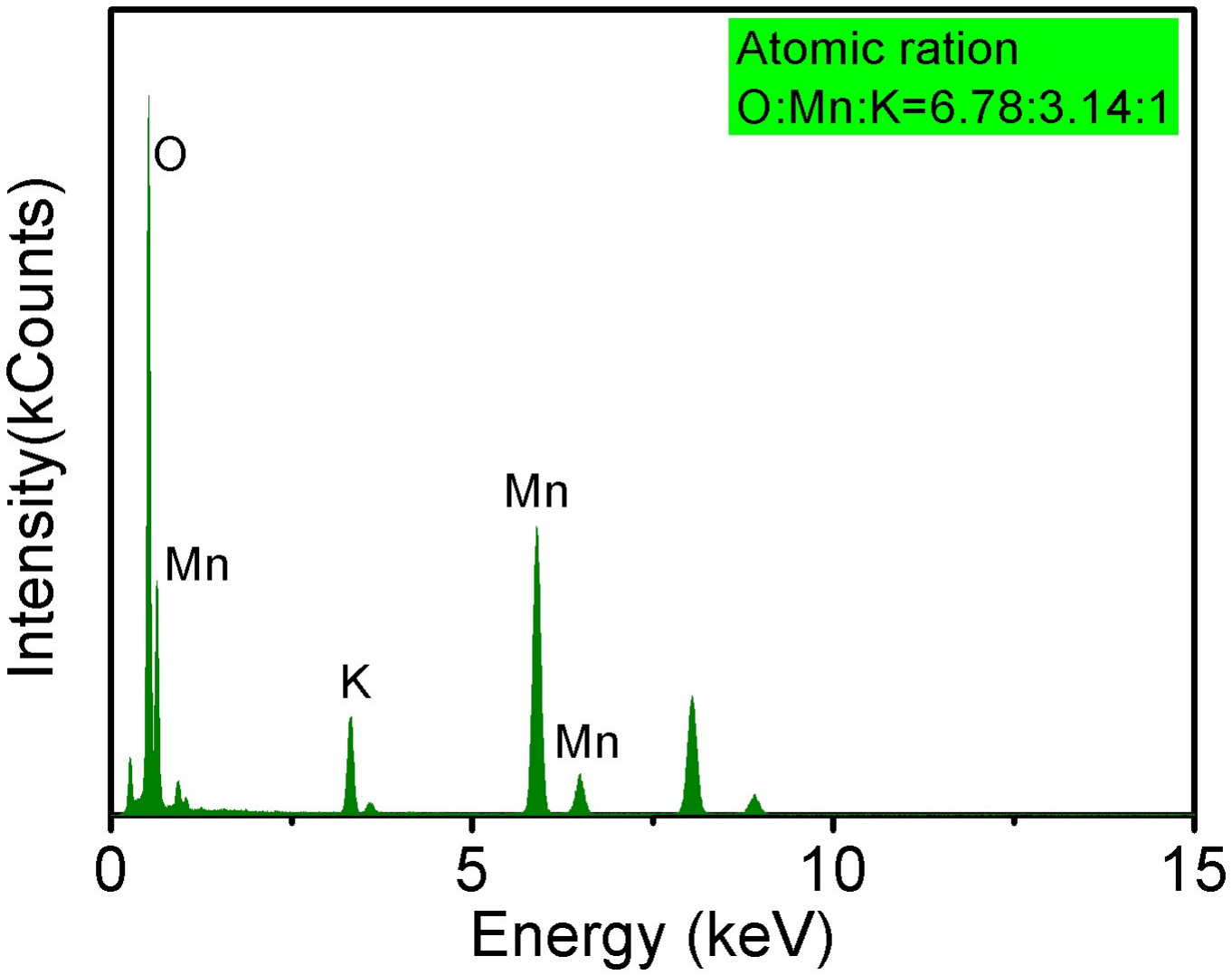

Figure.S5. The EDX spectrum of $K_{0.296}Mn_{0.926}O_2$.

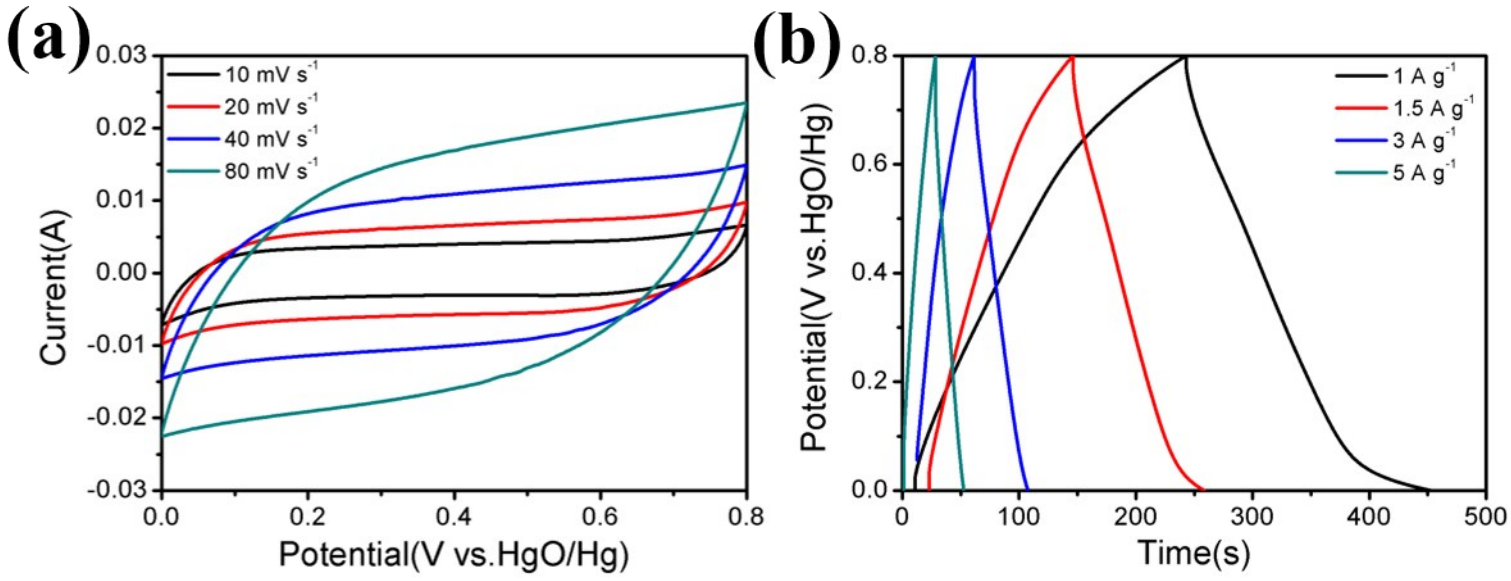

Figure.S6. (a) CV curves of commercial MnO_2 at the scan rate between 10 and 80 mV s^{-1}; (b) Galvanostatic charge-discharge curves of commercial MnO_2 at the current densities between 1 and 5 A g^{-1}.

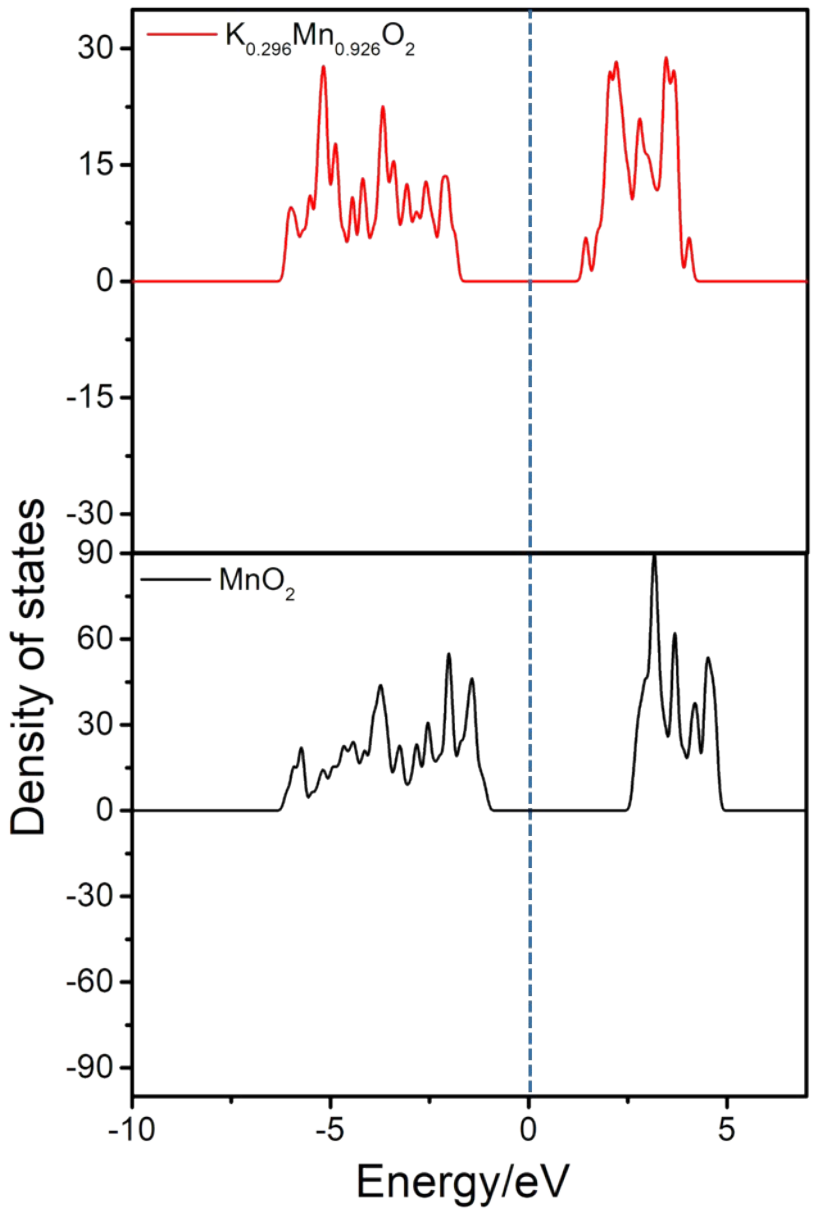

Figure.S7. Density of states (DOS) of the MnO_2 and as-prepared $K_{0.296}Mn_{0.926}O_2$ using density functional theory (DFT)

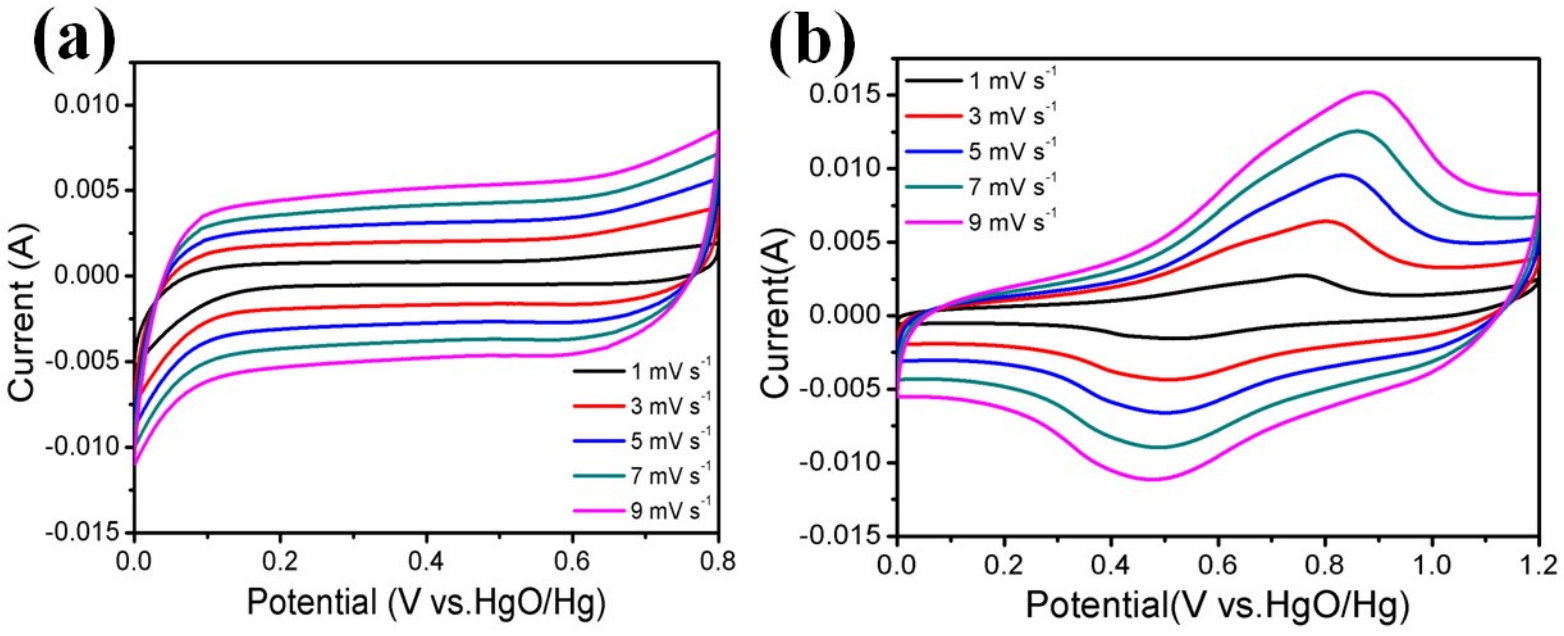

Figure.S8. (a), (b) CV curves of MnO_2 and as-prepared $K_{0.296}Mn_{0.926}O_2$ at the scan rate between 1 and 9 mV s^{-1}, respectively.

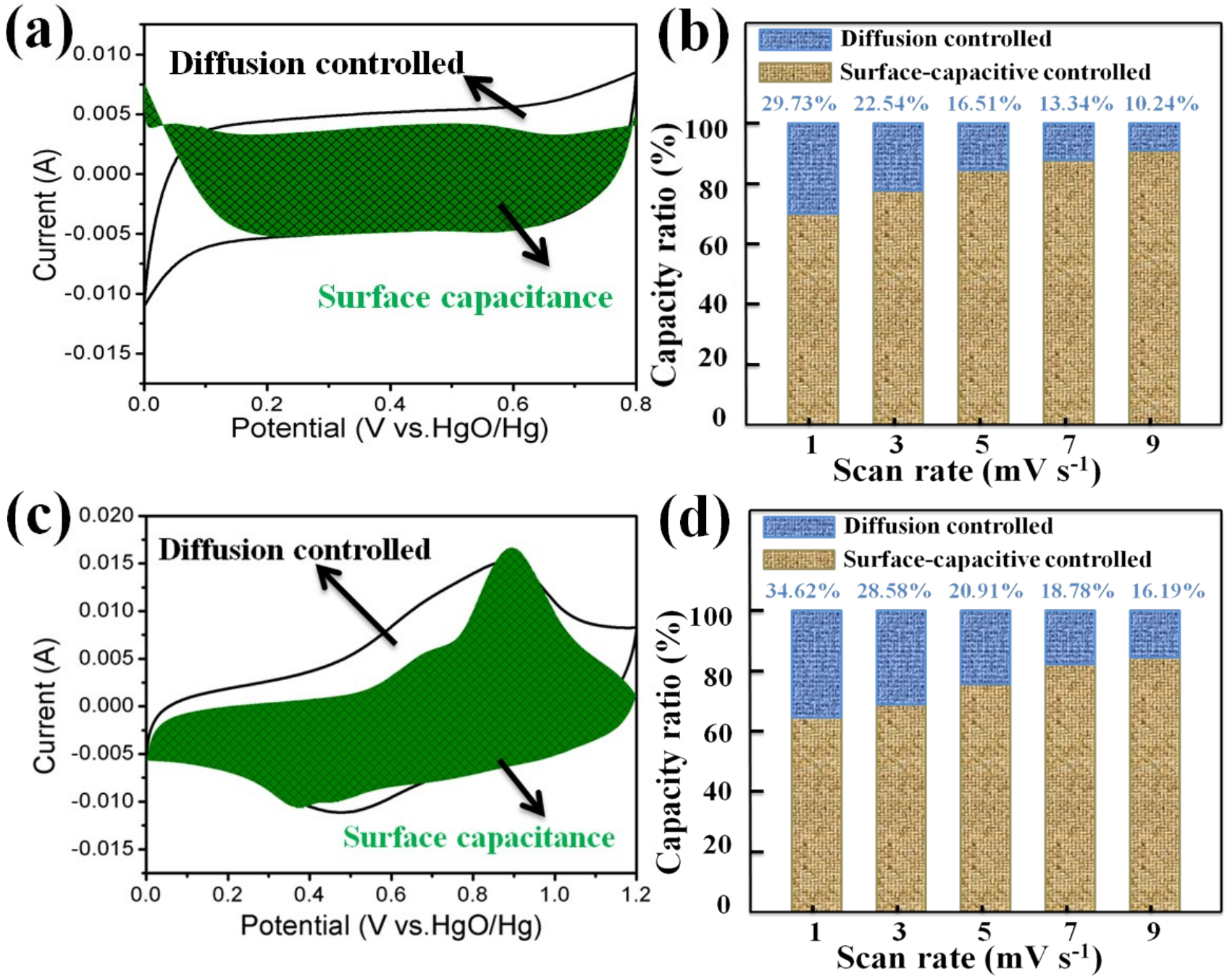

Figure.S9. (a), (c) The contribution of the different energy storage mechanism of the MnO_2 and $K_{0.296}Mn_{0.926}O_2$ at 9 mV s^{-1}; (b), (d) Percentage of diffusion-controlled and surface-capacitance for the MnO_2 and $K_{0.296}Mn_{0.926}O_2$ at various scan rates, respectively.

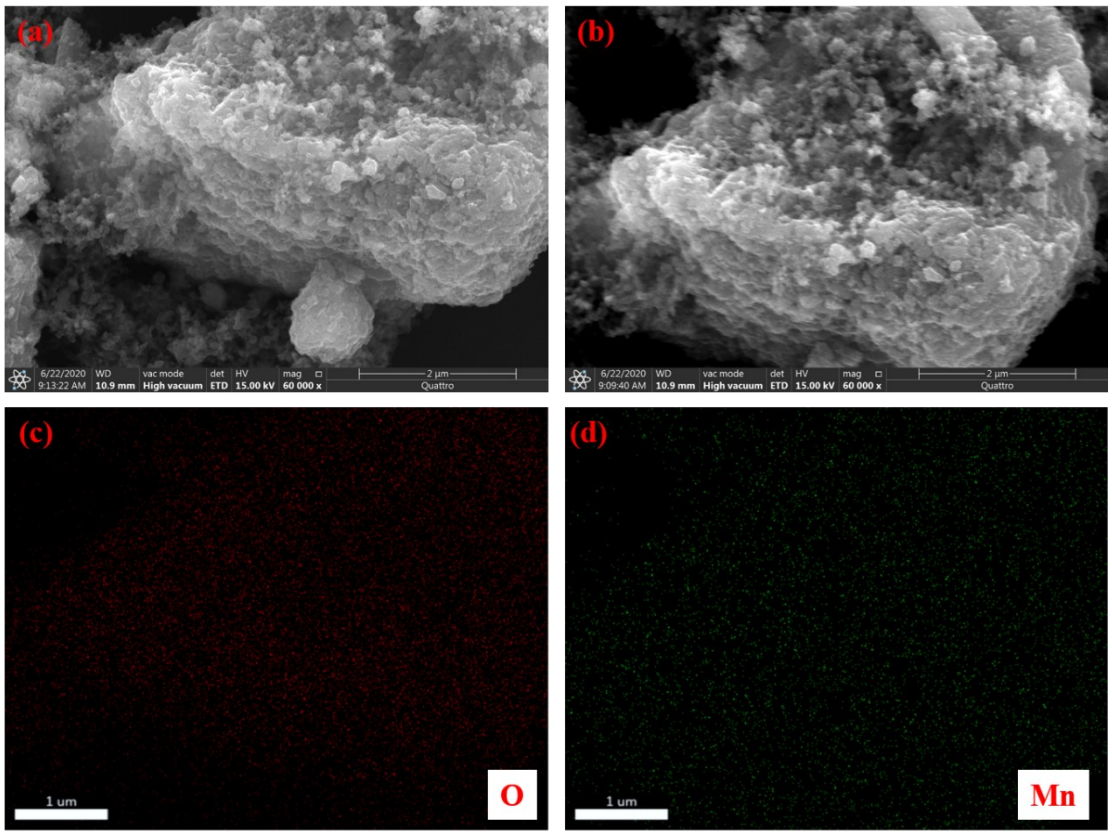

Figure S10. (a), (b) The SEM images of MnO_2 after cycling; (c), (d) EDS-mapping of Figure S9(b).

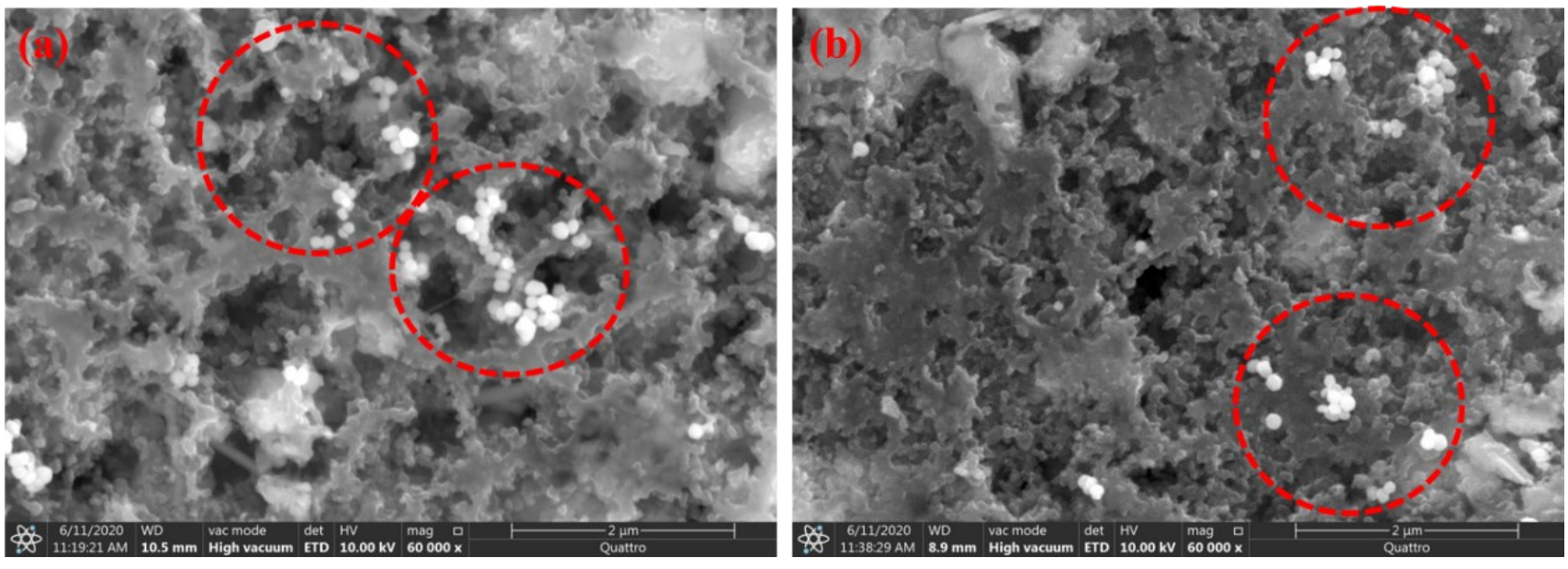

Figure S11. (a), (b) The SEM images of $K_{0.296}Mn_{0.926}O_2$ after cycling.

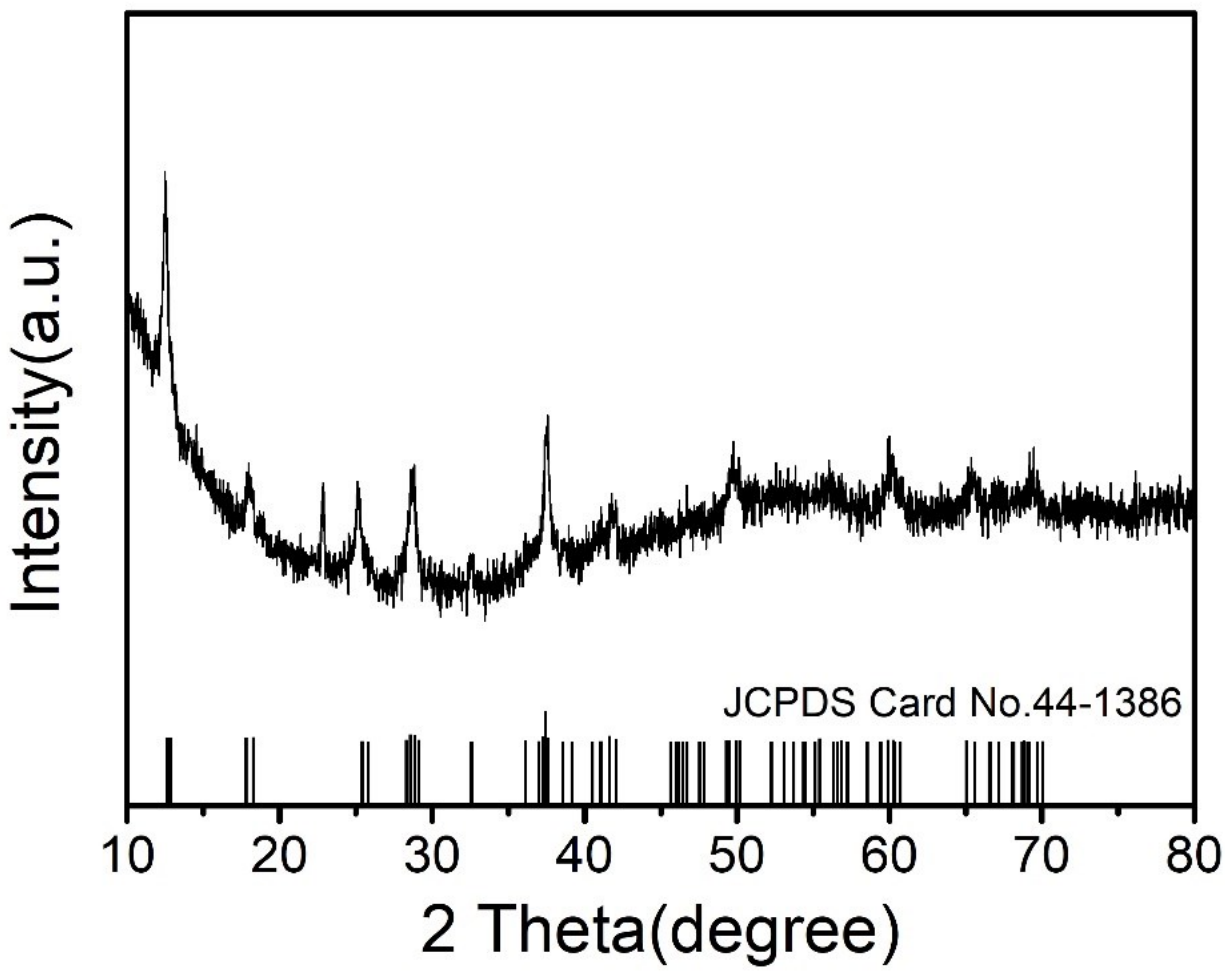

Figure S12. The XRD spectrum of $K_{0.296}Mn_{0.926}O_2$ after cycling.

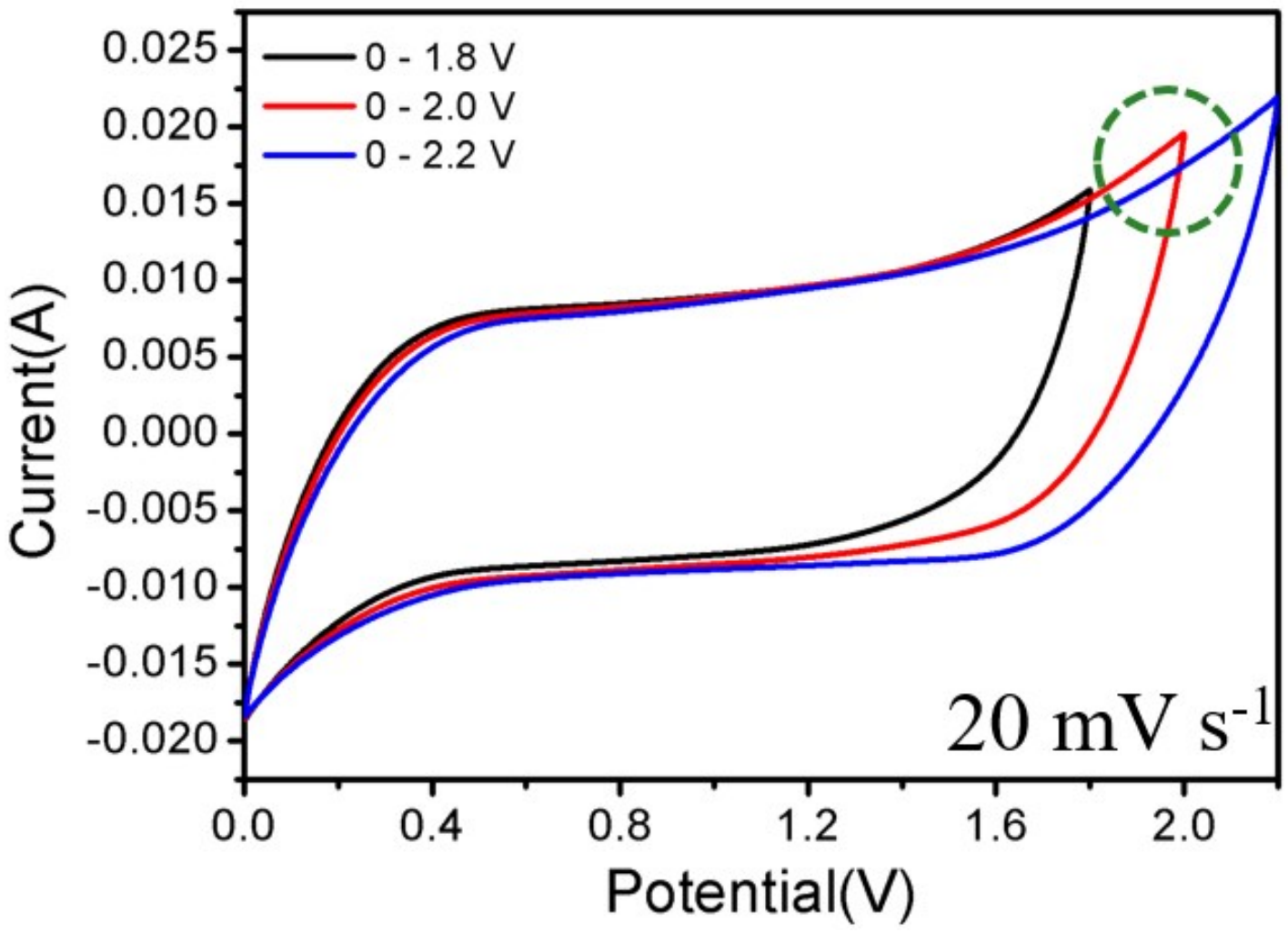

Figure.S13. CV curves of MnO_2//AC at different potentials at a scan rate of 20 mV s^{-1}.

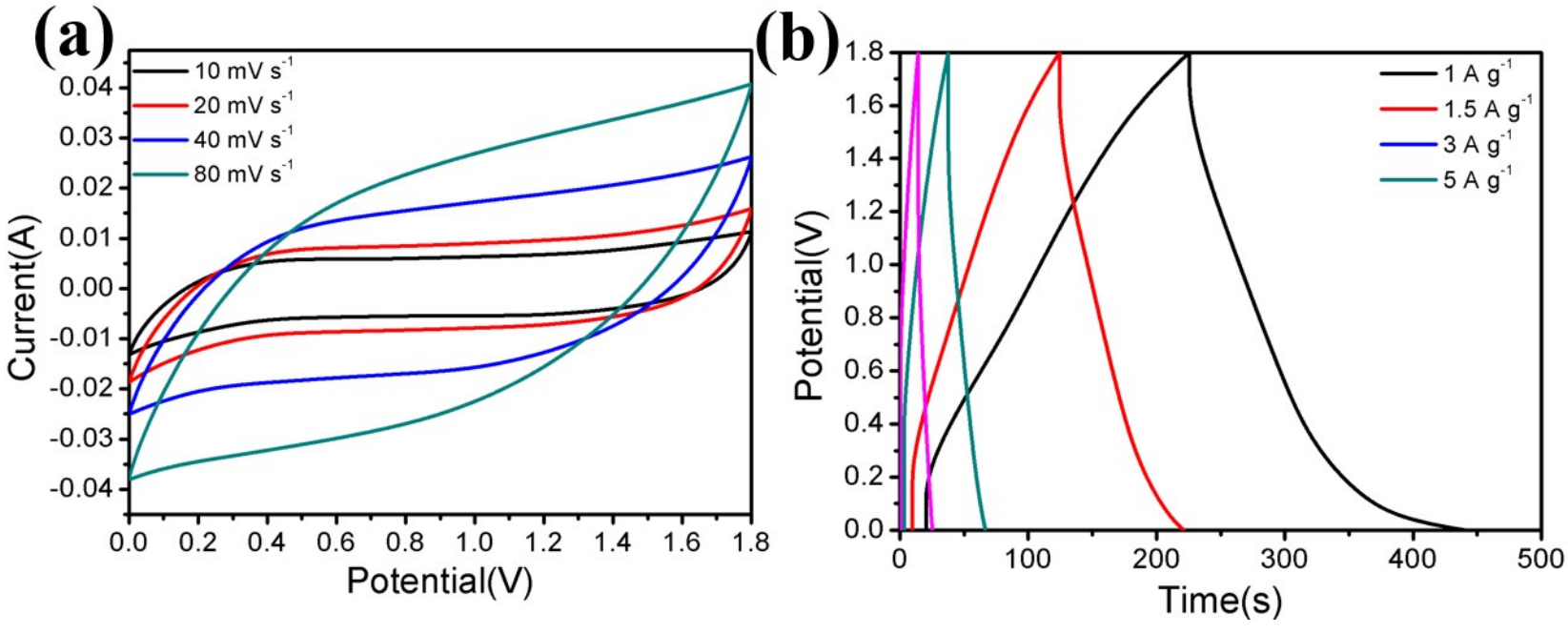

Figure.S14. (a) CV curves of MnO_2//AC at the scan rate between 10 and 80 mV s^{-1}; (b) Galvanostatic charge-discharge curves of MnO_2//AC at the current densities between 1 and 5 A g^{-1}.

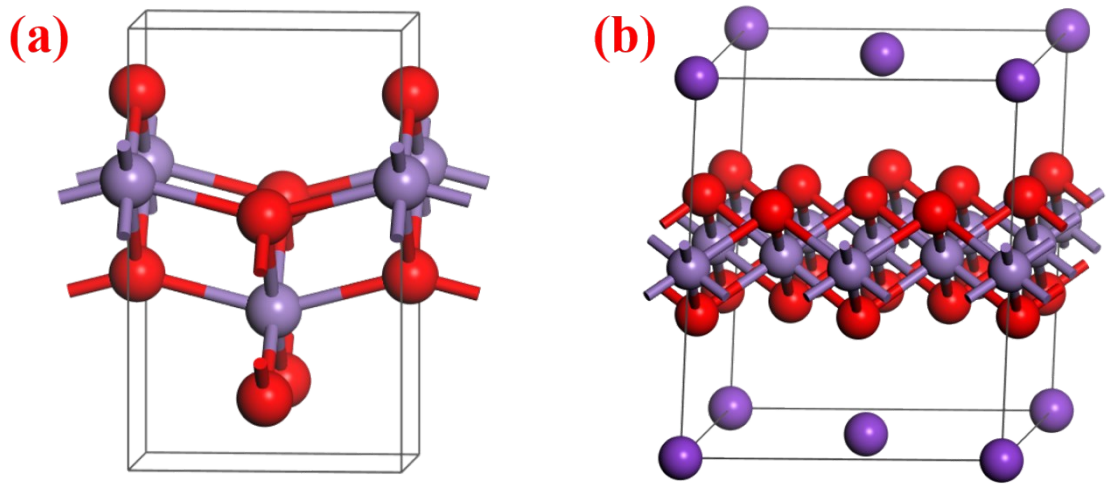

Figure. S15. (a), (b) The computational models of bulk MnO_2 and $K_{0.296}Mn_{0.926}O_2$, respectively.

Table S1. The comparative table of morphology, specific surface areas and average pore diameters of our prepared products with previously reported literature.

Samples	Morphology	Specific surface area ($m^2 g^{-1}$)	Average pore diameters (nm)	Device	Energy and power density	Reference
nanoporous carbon@$K_{0.5}Mn_2O_4$	nanosheets	/	/	NCMO//NC	60 Wh kg^{-1} at 1200 W kg^{-1}	[30]
ultrathin MnO_2	nanosheets	/	/	MnO_2/carbon fiber//graphene/carbon fiber	27.2 Wh kg^{-1} at 979.7 W kg^{-1}	[31]
MnO_2-CNT nanocomposite	nanoparticles	/	/	MnO_2-CNT//activated carbon	25 Wh kg^{-1} at 500 W kg^{-1}	[32]
MnO_2/graphene nano-composites	nanoparticles	332	/	MnO_2/graphene//graphene	35.2 Wh kg^{-1} at 7.4 kW kg^{-1}	[33]
graphene/MnO_2 composite	nanoparticles			graphene/MnO_2//activated carbon nanofibers	51.1 Wh kg^{-1} at 198 kW kg^{-1}	[34]
graphene-MnO_2	nanorods	43.8	2-5	graphene-MnO_2//densely stacked graphene	62.4 Wh kg^{-1} at 180 kW kg^{-1}	[35]
$K_{0.296}Mn_{0.926}O_2$	nanoparticles	52.4	3.7	$K_{0.296}Mn_{0.926}O_2$//AC	70 Wh kg^{-1} at 1200 kW kg^{-1}	This work